Supporting Information

Confined Growth of Pyridinic N-Mo_2C Sites on MXenes for Hydrogen Evolution

Hao Wang,[a1] Yanping Lin,[b1] Shuyuan Liu,[b1] Jianmin Li,[c] Liangmin Bu,[b] Jianmei Chen,[d] Xu Xiao,[e*] Jin-Ho Choi,[b] Lijun Gao,[b*] and Jong-Min Lee[a*]

[a.]School of Chemical and Biomedical Engineering, Nanyang Technological University, Singapore 637459, Singapore. E-mail: jmlee@ntu.edu.sg.
[b.]Soochow Institute for Energy and Materials Innovations, College of Energy, Soochow University, Suzhou 215006, China. E-mail: gaolijun@suda.edu.cn.
[c.]Department of Materials Science and Engineering, National University of Singapore, Singapore, 117576 Singapore.
[d.]Institute of Functional Nano and Soft Materials (FUNSOM), Jiangsu Key Laboratory for Carbon-Based Functional Materials & Devices, Soochow University, Suzhou 215123, China.
[e.]A.J. Drexel Nanomaterials Institute and Department of Materials Science and Engineering, Drexel University, Philadelphia, 19104, United States. E-mail: xx58@drexel.edu
[1]These authors contribute equally to this work.

Experimantal

Synthesis of $Ti_3C_2T_x$ MXene: $Ti_3C_2T_x$ MXene was synthesized by selective etching of Al from Ti_3AlC_2 powder (Jilin 11 Technology Co., Ltd.). Firstly, 2 g of lithium fluoride (LiF, Sigma-Aldrich) was fully dissolved in 20 mL of 9 M hydrochloric acid (HCl, Fisher Chemical) followed by slowly adding 2 g of Ti_3AlC_2 powder and stirring for 24 h at 35 °C. Then the mixture was washed with deionized water and centrifuged at 3500 rpm for several times until the pH reached ~6, then multilayered $Ti_3C_2T_x$ was obtained. The delaminated $Ti_3C_2T_x$ flakes were prepared by sonicating the above multilayered $Ti_3C_2T_x$ aqueous solution for 1 h (Branson Ultrasonic Cleaner, 40 kHz) in an ice bath under argon gas protection. Then, the solution was centrifuged at 3500 rpm for 1 h, and the dark supernatant was kept for further use.

Synthesis of Mo-PDA/$Ti_3C_2T_x$, Mo-PDA, and PDA/ $Ti_3C_2T_x$: To prepare Mo-PDA/$Ti_3C_2T_x$, 20 mg of $Ti_3C_2T_x$ MXene and 50 mg of ammonium molybdate tetrahydrate (Sigma-Aldrich) was dissolved in 10 mL of deionized water, and 50 mg of dopamine hydrochloride (Sigma-Aldrich) was dissolved in 20 mL of ethanol (Sigma-Aldrich). Then the two solutions were mixed and subsequently, 0.2 mL of ammonium hydroxide (Sigma-Aldrich) was quickly added into the mixture solution. After stirring for 1 h, Mo-PDA/$Ti_3C_2T_x$ was obtained by washing with ethanol and centrifugation. Mo-PDA was prepared by the same procedure without adding $Ti_3C_2T_x$ MXene while PDA/$Ti_3C_2T_x$ was obtained by the same method without adding ammonium molybdate tetrahydrate. All the samples were lyophilized for further use.

Synthesis of $Mo_2C/Ti_3C_2T_x$@NC, Mo_2C@NC, and $Ti_3C_2T_x$@NC: These three samples were prepared by annealing Mo-PDA/$Ti_3C_2T_x$, Mo-PDA, and PDA/$Ti_3C_2T_x$ at 750 ^oC for 3h under argon atmosphere with a heating rate of 2 ^oC min^{-1}, respectively. Pristine $Ti_3C_2T_x$ MXene was also treated with the same progress for comparison.

Characterizations: The morphology and microstructure of the samples were characterized by SEM (Hitachi SU8010), TEM (FEI Titan Themis G2, acceleration voltage 30-300 kV) and N_2 adsorption/desorption isotherm analyzer (Tristar II 3020). The structures and compositions were investigated by XRD (Bruker D8 Advance Diffractometer), Raman spectroscopy (Horiba, HR Evolution, 532 nm), XPS (Escalab 250Xi Spectrophotometer using a monochromatic Al Kα X-ray source). Inductively coupled plasma optical emission spectroscopy (ICP-OES) (OPTIMA 8000, PerkinElmer) was used to analyze the content of molybdenum in the samples.

Electrochemical measurements: All the electrochemical measurements were performed in a three-electrode system on the electrochemical workstation (CHI 660E) in Ar-saturated 0.5 M H_2SO_4 at room temperature. A glassy carbon electrode (3 mm in diameter), Ag/AgCl KCl-saturated electrode and a graphite rod (Alfa Aesar) were used as working electrode, reference electrode and counter electrode, respectively. The HER activities of the samples in neutral and basic media were measured in 1M PBS and 1M KOH, respectively, with Ag/AgCl KCl-saturated electrode and KOH-saturated Hg/HgO electrode as reference electrode, respectively. All the LSV curves were measured with a scan rate of 2 mV s^{-1}. All the potentials here are without iR correction and were calibrated with respect to the reversible hydrogen electrode (RHE) according to the Nernst equations: E (V vs RHE) = E (V vs Ag/AgCl) + 0.197 + 0.0592 × pH or E (V vs RHE) = E (V vs Hg/HgO) + 0.098 + 0.0592 × pH. The catalyst (2 mg) was dispersed in a mixture solution of 450 μL of ethanol and 50 μL of Nafion 117 (Sigma Aldrich, 5 wt%) by sonication for 30 min. Then, 5 μL of as-prepared dispersion was pipetted onto glassy carbon electrode with a mass loading of 0.285 mg cm^{-2} and dried naturally. To estimate the electrochemical active surface area (ESCA) of the samples, cyclic voltammograms (CV) were tested by measuring double-layer capacitance (C_{dl}) under the potential window of 0.2 and 0.3 V vs. RHE with various scan rates of 10-100 mV s^{-1}. The Nyquist plots were measured at an overpotential of 100 mV with frequencies ranging from 100 kHz to 0.1 Hz and an alternating current voltage of 5 mV. The cycling stability of $Mo_2C/Ti_3C_2T_x$@NC was recorded by CV under the potential window of 0.1 and -0.2 V vs. RHE for 1000 cycles while the long-term stability was performed at an overpotential of 100 mV for 30 h.

DFT calculations: Our first-principles density functional theory (DFT) calculations were performed using the projector-augmented-wave (PAW) method and the Perdew-Burke-Ernzerhof (PBE) exchange-correlation functional as implemented in the Vienna Ab-initio Simulation Package (VASP).[1-3] To include the effects of long-range van der Waals (vdW) interactions, a semi-classical dispersion correction scheme (DFT-D3) was employed.[4] A plane-wave basis was employed with a kinetic energy cutoff of 550 eV, and k-space integration was done with 3 × 3 meshes in the 2D Brillouin zones. Electron density was self-consistently converged with an energy threshold of 10^{-6} eV. All atoms were allowed to completely relax until the residual forces exerted on each atom were less than 0.02 eV/Å during the structural optimization.

We constructed the correlative theoretical models to simulate the HER properties in C-graphitic N, C-pyridinic N, Mo_2C (001), MXence, Mo_2C@C-graphitic N, Mo_2C@C-pyridinic N, MXence@C-graphitic N, and MXence@C-pyridinic N systems for comparative. Mo_2C (001) surface is modeled with four layers of atoms in Mo-termination. The composited Mo_2C@C-graphitic N and Mo_2C@C-pyridinic N models were constructed by covering the respective C-graphitic N and C-pyridinic N layers on the (001) facet of the Mo_2C slab. The supercells for Mo_2C@C-graphitic N and Mo_2C@C-pyridinic N are in rectangular lattice, and the corresponding lattice constant is a = 12.03 Å, b = 10.36 Å. The supercells for MXence@C-graphitic N and MXence@C-pyridinic N are in hexagonal lattice with a = b = 12.13 Å. For the systems that involve Mo_2C (001), the top two layers of Mo_2C (001) and graphene (plus adsorbate H) are allowed to relax, while the rest of the slab remained fixed. The Gibbs free energy for hydrogen adsorption (ΔG_{H*}) was calculated by a formula $\Delta G_{H*} = \Delta E_H + \Delta E_{ZPE} - T\Delta S_H$, where ΔE_H, ΔE_{ZPE}, and ΔS_H represent the

hydrogen adsorption energy, zero-point energy difference, and entropy difference between the adsorbed state and the gas phase, respectively.

Note S1. Determination of Mo content in samples by ICP-OES.

The method of determination of Mo_2C loading in $Mo_2C/Ti_3C_2T_x$@NC using ICP-OES elemental analysis is according to literature reported previously.[5] 5 mg of sample was digested by 1 mL of aqua regia solution. Then 0.2 mL of the solution was diluted to 100 mL volumetric flask. The weight percentage (wt%) of Mo_2C (W_{Mo2C}) in sample can be calculated as following,

$$W_{Mo2C} = C_{Mo} \times V / m_{total} / M_{Mo} \times M_{Mo2C}/2 \times 100\% \quad (1)$$

Where C_{Mo} is the measured concentration of Mo ions in the solution [mg L^{-1}]; V is the total volume of the prepared sample solution in the volumetric flask [L]; m_{total} is the mass of total $Mo_2C/Ti_3C_2T_x$@NC sample used for digestion [0.005 g]; M_{Mo} is the molar mass of Mo [95.94 g mol^{-1}]; M_{Mo2C} is the molar mass of Mo_2C [203.88 g mol^{-1}].

C_{Mo} for $Mo_2C/Ti_3C_2T_x$@NC and Mo_2C@NC is determined to be 3.999 and 5.697 mg L^{-1}. Thus, the W_{Mo2C} is calculated to be 42.5 wt% and 60.5 wt%.

Note S2. Calculation of electrochemically active surface area (ECSA) of catalysts.

The ECSA of catalysts is estimated by the electrochemical double layer capacitance (C_{dl}), assuming that the quantities are linearly proportional.[6] The cyclic voltammetry measurements are conducted between the potentials of 0.2 and 0.3 V vs RHE at seven different scan rates (10, 20, 30, 40, 50, 60, 70, 80, 90, 100 mV s^{-1}). The specific capacitance could be calculated from the scan rate dependence of capacitive current density at a

potential at 0.25 V, where the slope of the Δj vs scan rate curve is just twice of the C_{dl}. The specific capacitance for a flat surface depending on the electrode materials is generally found to be in the range of 20-60 μF cm^{-2}. In view of the similarity of the surface capacitances in the same aqueous electrolyte, we thus assume a moderate value of 40 μF cm^{-2} for the following calculations of ECSA.

$$ECSA = C_{dl} / 40\ \mu F\ cm^{-2} \qquad (2)$$

The ECSA for $Mo_2C/Ti_3C_2T_x$@NC (24.15 mF cm^{-2}) and Mo_2C@NC (21.56 mF cm^{-2}) are estimated to be 603.75 and 539 cm^2.

Note S3. Calculation of per-site turnover frequency (TOF) of catalysts.

TOF refers the number of H_2 molecules evolved per second per active sites, which can be calculated as following,[7]

$$TOF = j \times A \times N_A / (n \times F) / S \qquad (3)$$

Where j is the current density from Figure 5a (A $cm^{-2}_{electrode}$); A is the the geometric surface area of the electrode disk (0.07 cm^{-2}); NA is the Avogadro's constant (6.02×10^{23} per mol); n is the number of electrons transferred per molecule (2 for H_2 molecule); F is the Faraday's constant (96485 C per mol electrons); S is the number of active sites. Here, all the Mo atoms in the samples are considerd as active sites which are determined by ICP-OES.

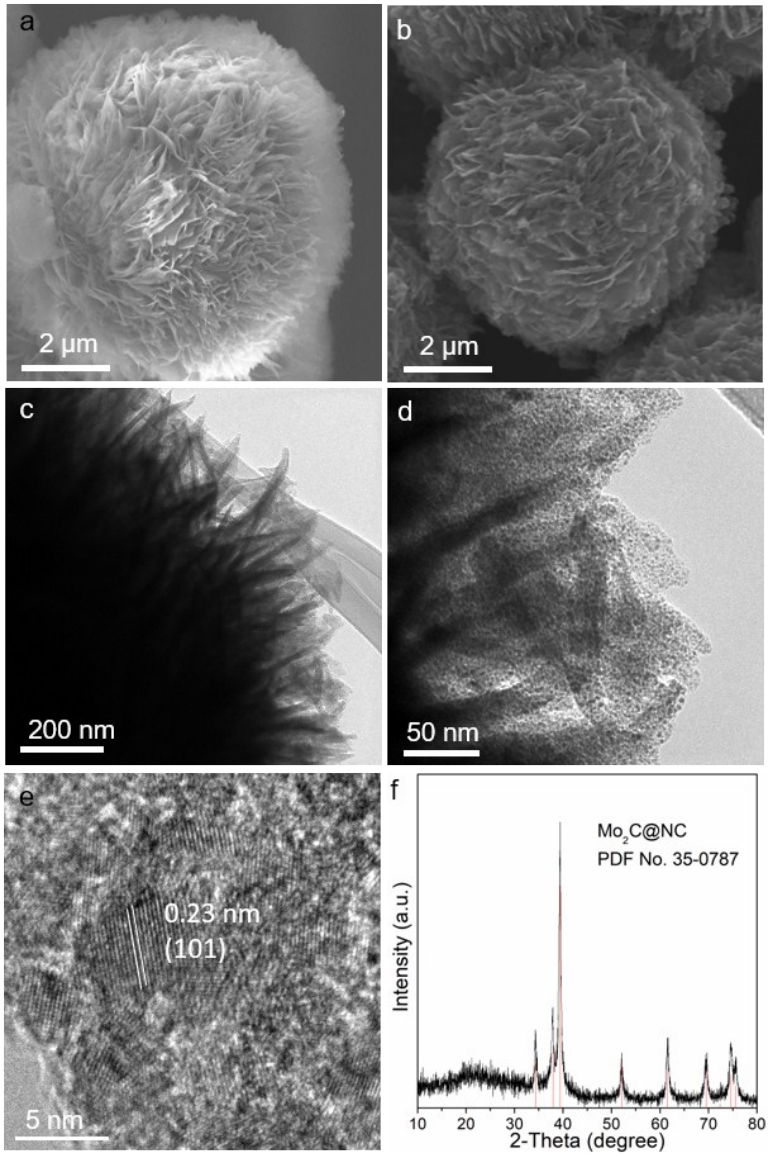

Fig. S1. SEM images of (a) Mo-PDA and (b) Mo_2C@NC. (c, d) TEM, (e) HRTEM images and (f) XRD pattern of Mo_2C@NC. After the carburization, the hierarchical architecture is well reserved that numerous Mo_2C nanodots are anchored on carbon nanosheets. The lattice fringes with a spacing of 0.23 nm are in good agreement with the d-spacing of the β-Mo_2C (111) plane. The typical XRD pattern of Mo_2C@NC is well assigned to the Mo_2C crystal phase (PDF No. 35-0787).

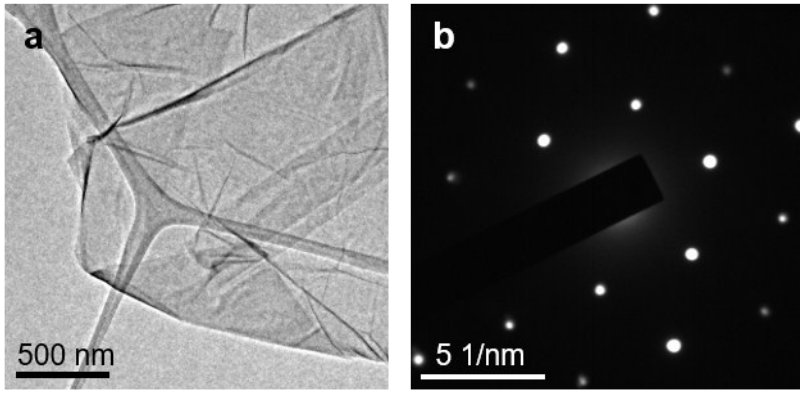

Fig. S2. TEM image (a) and corresponding SAED pattern (b) of pristine $Ti_3C_2T_x$ MXene.

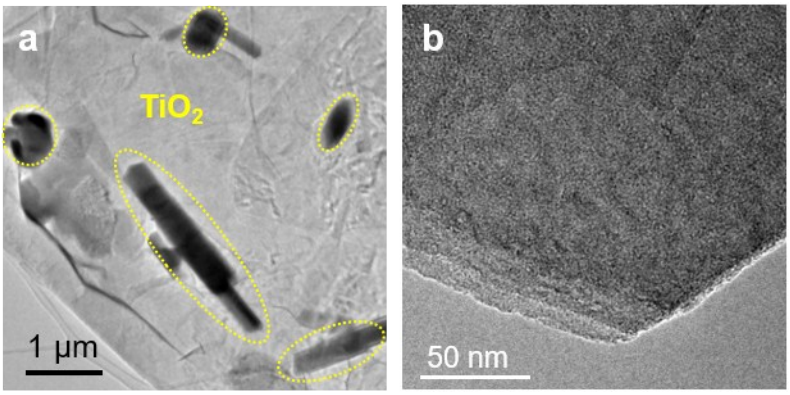

Fig. S3. TEM images of (a) annealed $Ti_3C_2T_x$ MXene and (b) $Ti_3C_2T_x$@NC.

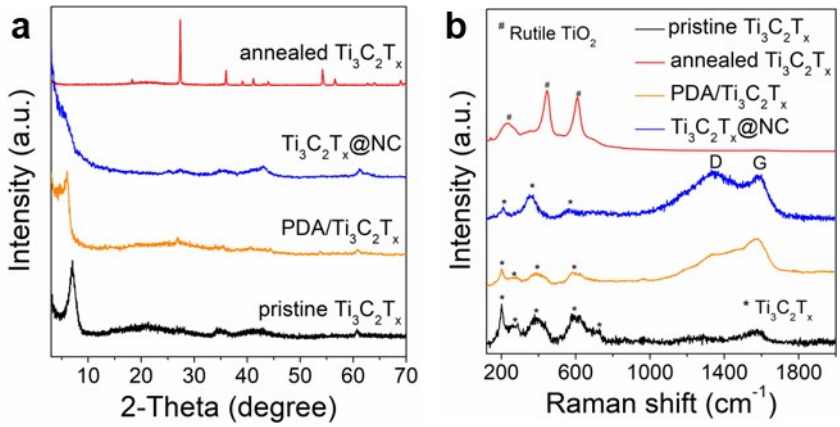

Fig. S4. XRD pattens (a) and Raman spectra (b) of various samples.

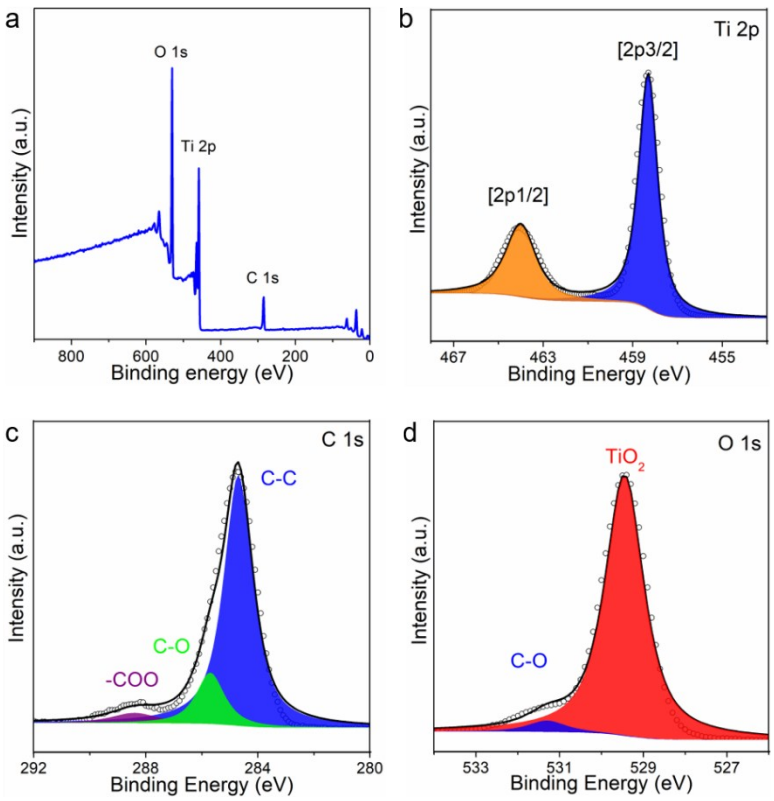

Fig. S5. (a) XPS full scan of annealed $Ti_3C_2T_x$ MXene. XPS high-resolution spectra of (b) Ti 2p, (c) C 1s and (d) O 1s. The XPS analysis reveals that annealed $Ti_3C_2T_x$ MXene consists of TiO_2 and carbon.

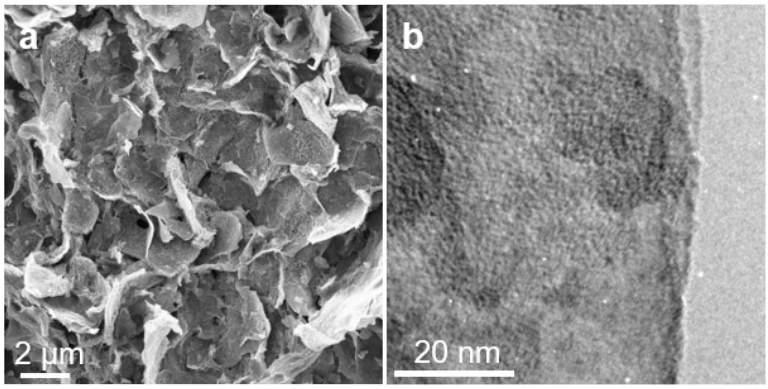

Figure S6. (a) SEM and (b) TEM images of Mo-PDA/$Ti_3C_2T_x$.

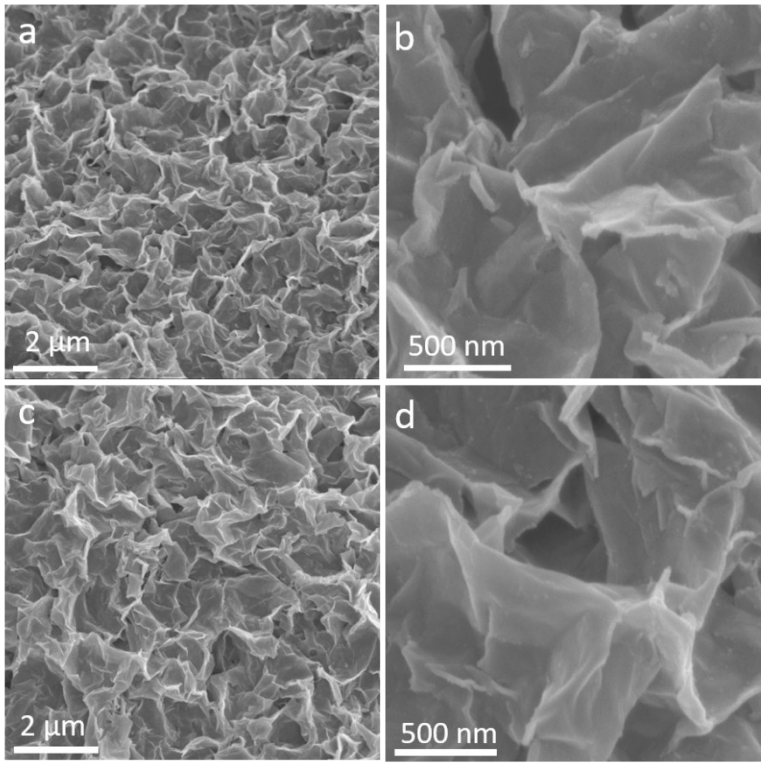

Fig. S7. SEM images of (a, b) $Mo_2C/Ti_3C_2T_x$@NC and (c, d) $Ti_3C_2T_x$@NC.

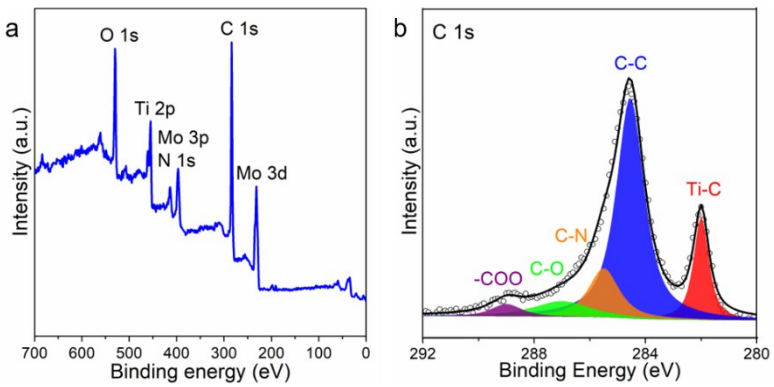

Fig. S8. (a) XPS full scan and (b) C 1s spectrum of $Mo_2C/Ti_3C_2T_x$@NC.

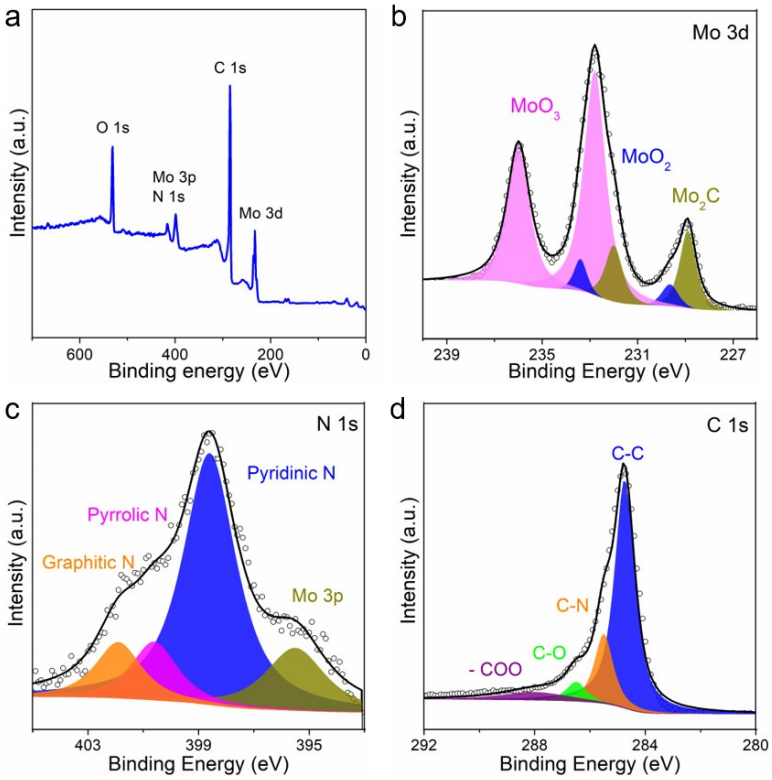

Fig. S9. (a) XPS full scan of Mo_2C@NC. XPS high-resolution spectra of (b) Mo 3d, (c) N 1s and (d) C 1s. The surface of the Mo_2C@NC is composed of Mo, N, C, and O elements. The Mo 3d spectrum shows the peaks located at the binding energy of 228.9 and 231.9 eV ($3d_{5/2}$ and $3d_{3/2}$, respectively) are assigned to Mo_2C while the peaks at 235.9, 233.5, 235.0 and 232.4 eV can be assigned to Mo^{6+} $3d_{3/2}$, Mo^{6+} $3d_{5/2}$, Mo^{4+} $3d_{3/2}$ and Mo^{4+} $3d_{5/2}$, respectively. The N 1s XPS spectrum shows that the spectrum can be mainly fitted into three peaks, including pyridinic N, pyrrolic N and graphitic N. The C 1s spectrum is deconvoluted into four peaks related to C-C, C-N, C-O and -COO.

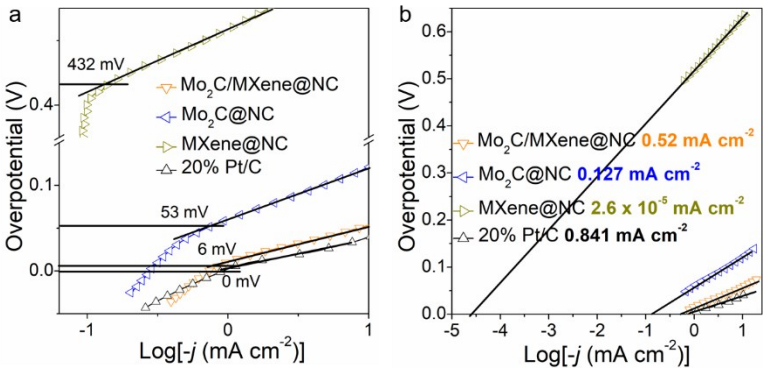

Fig. S10. (a) Tafel plots in the region of low current densities, where the inflection point of the linear part is denoted as the onset overpotentials of the catalysts. (b) Tafel plots with extrapolating curves for the samples. The section points on X-Axis at η=0 are determined to be -0.075, -0.896, and -4.585 for Pt/C, $Mo_2C/Ti_3C_2T_x$@NC, Mo_2C@NC, and $Ti_3C_2T_x$@NC, respectively, corresponding the the exchange current density of 0.841, 0.52, 0.127, 0.076 and 2.6×10^{-5} mA cm^{-2}.

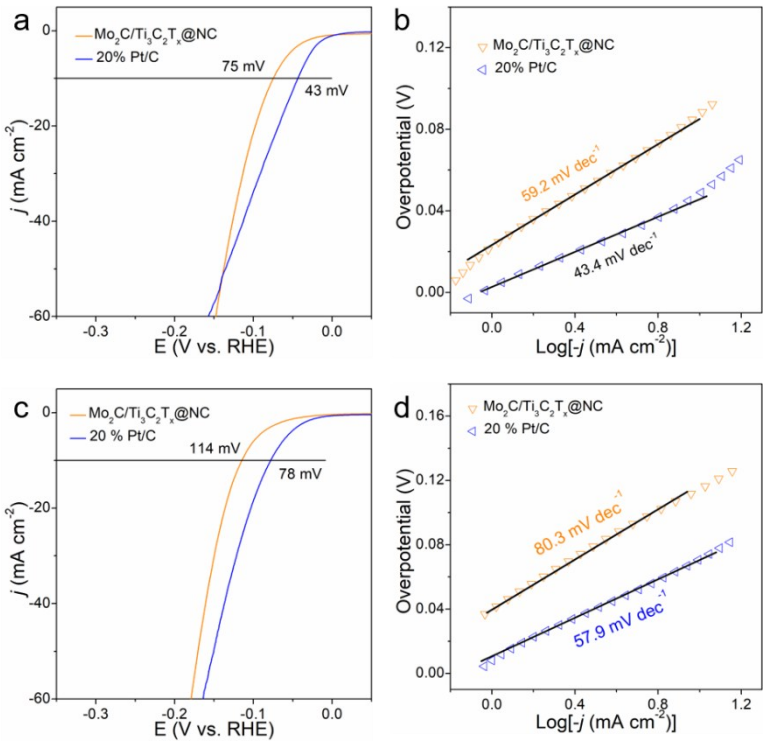

Fig. S11. HER perfromance of $Mo_2C/Ti_3C_2T_x$@NC and 20% Pt/C in alkaline (a, b) and neutral media (c, d).

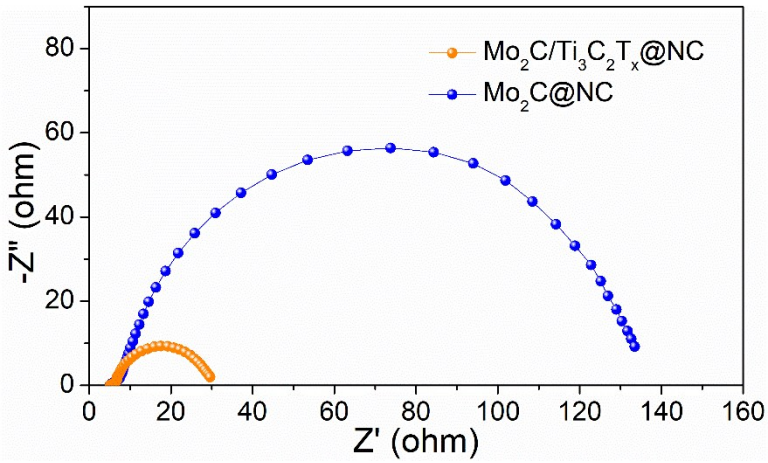

Fig. S12. EIS spectra of $Mo_2C/Ti_3C_2T_x$@NC and Mo_2C@NC at the overpotential of 100 mV. Compared with the Nyquist plot of Mo_2C@NC, that of $Mo_2C/Ti_3C_2T_x$@NC shows a much smaller semicircle, suggesting that $Mo_2C/Ti_3C_2T_x$@NC has lower charge transfer resistance during HER process.

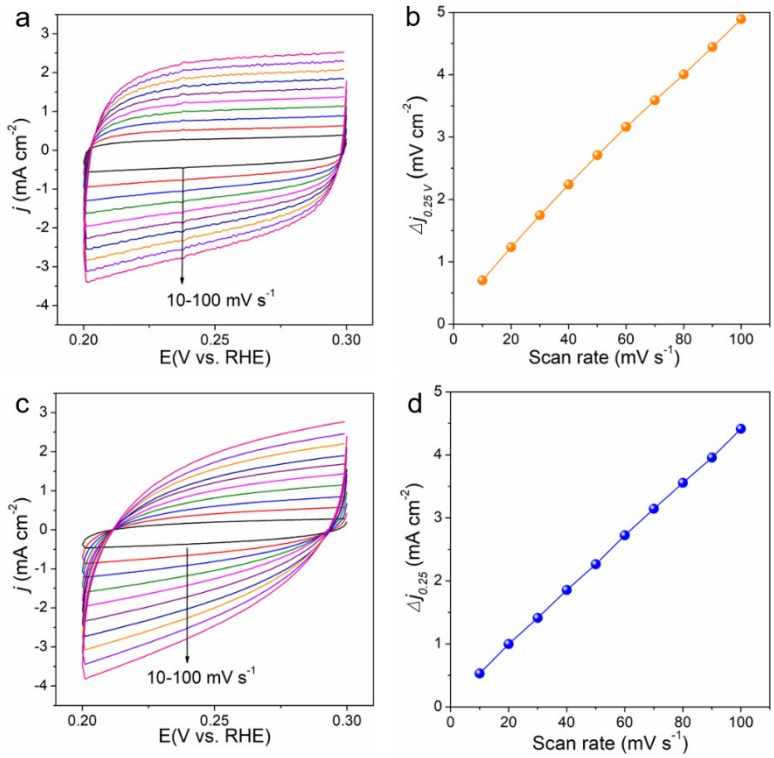

Fig. S13. CV curves of (a) $Mo_2C/Ti_3C_2T_x$@NC and (c) Mo_2C@NC under different scan rates from 10 to 100 mV s^{-1}. Capacitive current at 0.25 V vs. RHE as a function of scan rate for (b) $Mo_2C/Ti_3C_2T_x$@NC and (d) Mo_2C@NC.

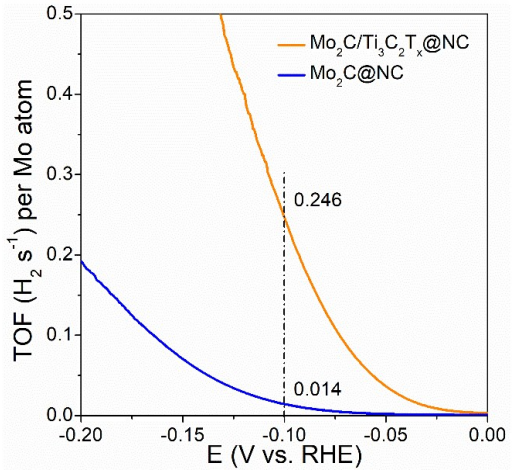

Fig. S14. TOF curves of $Mo_2C/Ti_3C_2T_x$@NC and Mo_2C@NC.

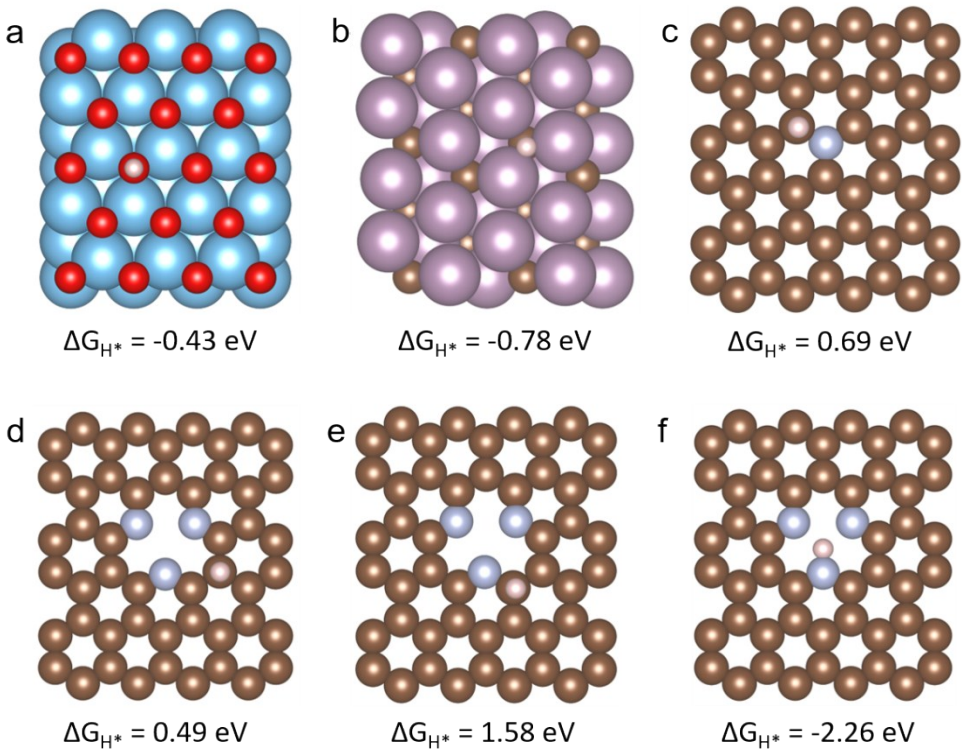

Fig. S15. The theoretical models used in DFT calculations and the adopted adsorption sites of H* on the surface of these models: (a) $Ti_3C_2T_x$; (b) Mo_2C; (c) g-N-C; (d-f) p-N-C.

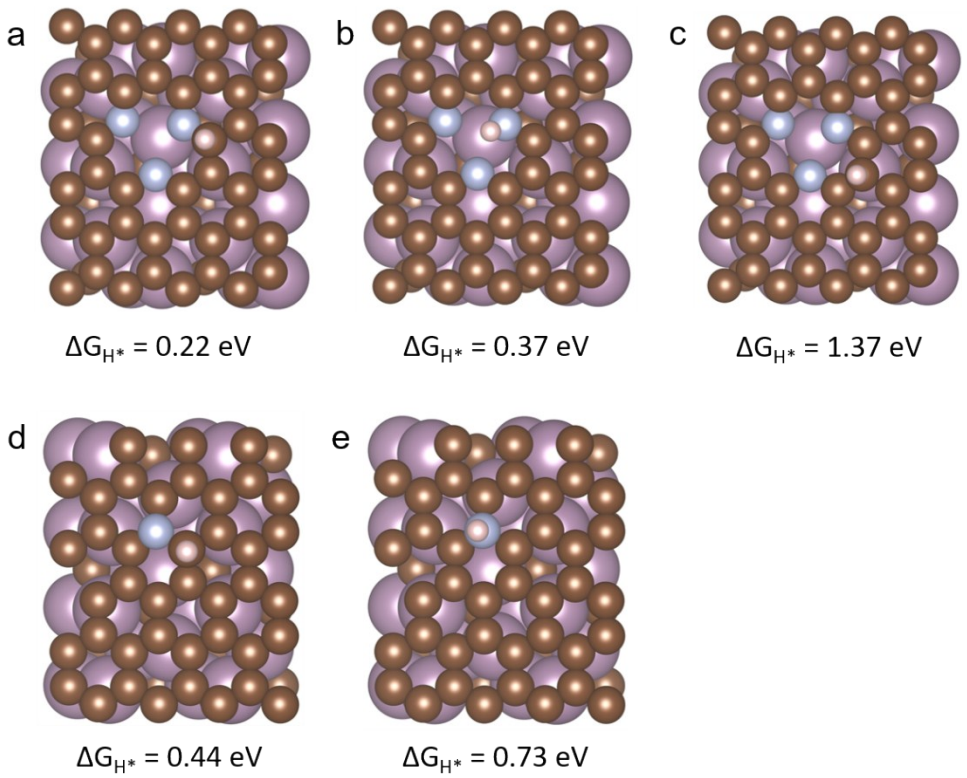

Fig. S16. The theoretical models used in DFT calculations and the adopted adsorption sites of H* on the surface of these models: (a-c) Mo_2C@p-N-C; (d, e) Mo_2C@g-N-C.

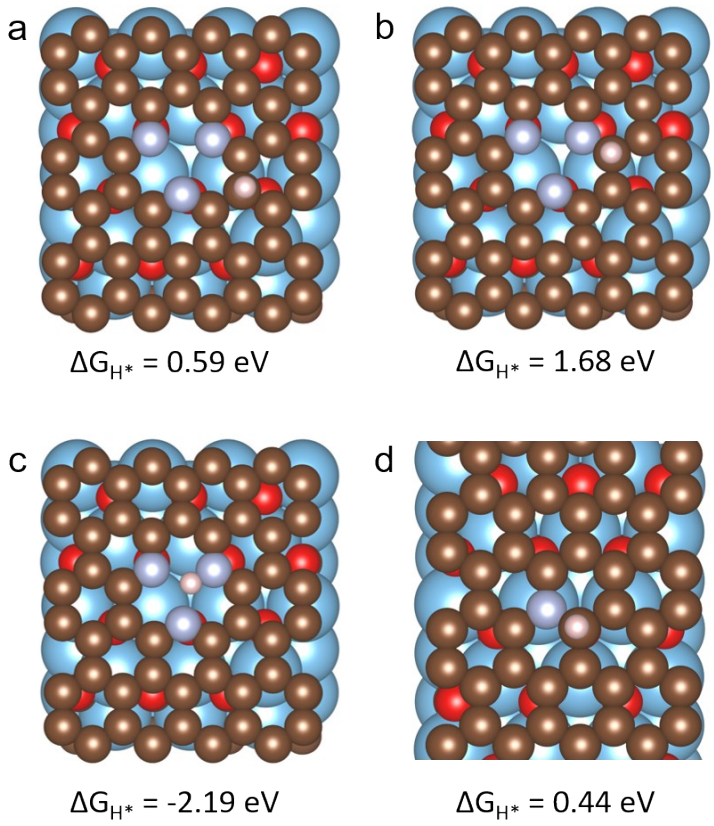

Fig. S17. The theoretical models used in DFT calculations and the adopted adsorption sites of H* on the surface of these models: (a-c) $Ti_3C_2T_x$@p-N-C; (d) $Ti_3C_2T_x$ @g-N-C.

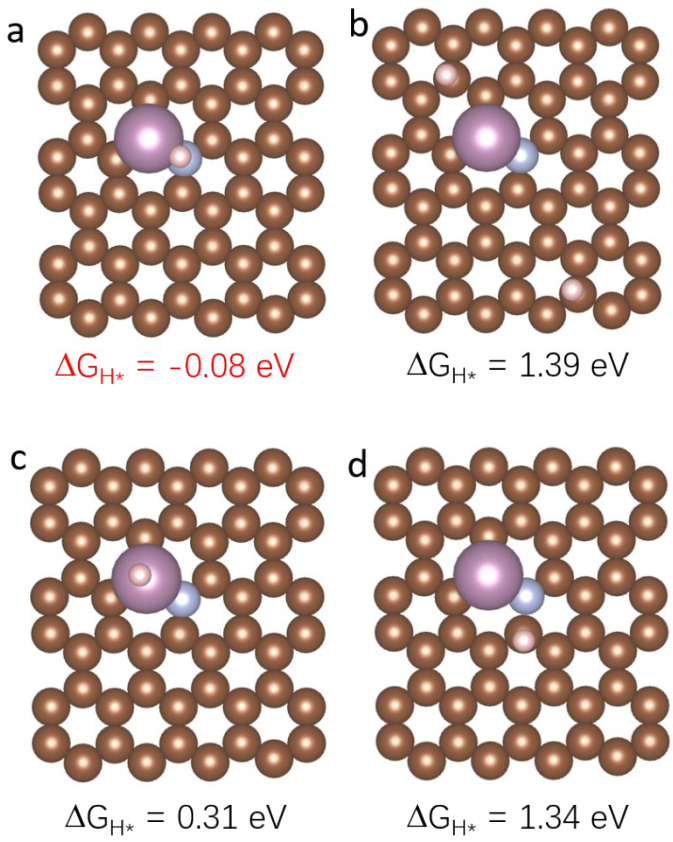

Fig. S18. The theoretical models used in DFT calculations and the adopted adsorption sites of H* on the surface of Mo-N-C structure.

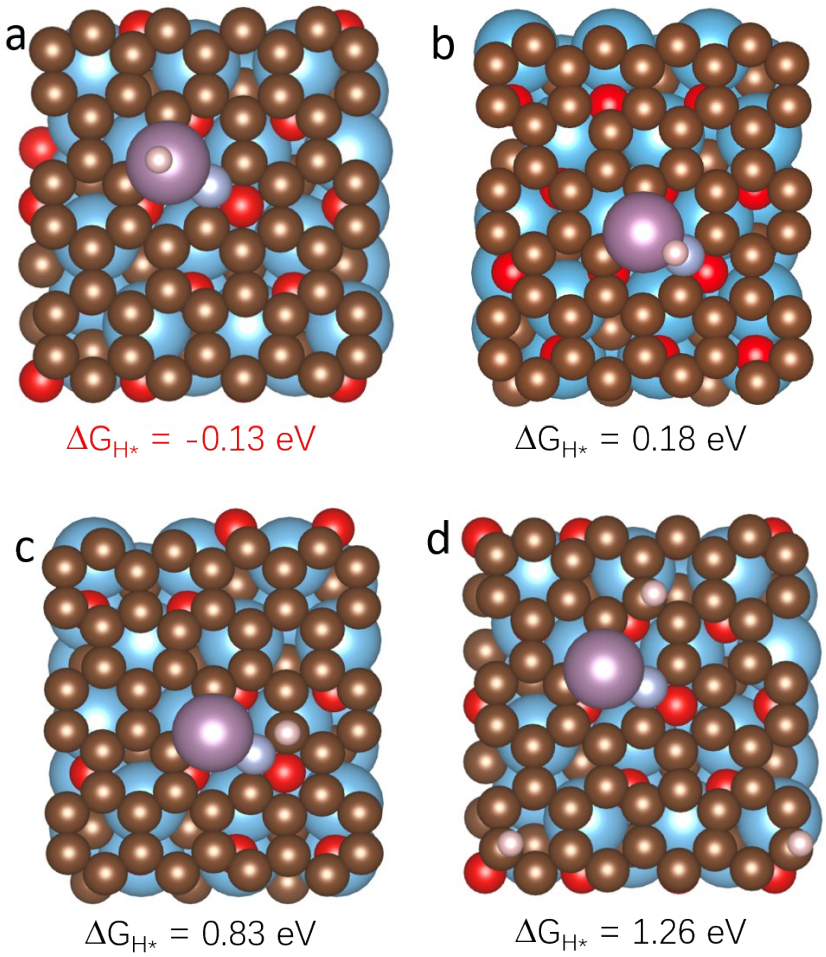

Fig. S19. The theoretical models used in DFT calculations and the adopted adsorption sites of H* on the surface of Mo-N-C/$Ti_3C_2T_x$ heterostructure.

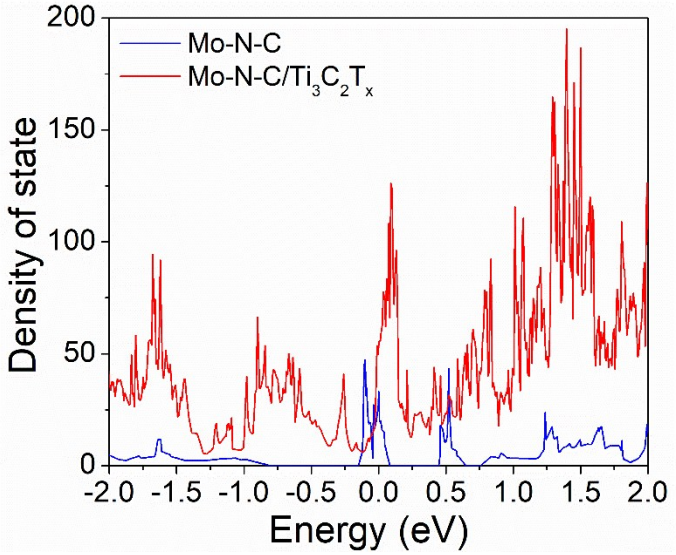

Figure S20. Calculated density of states for Mo-N-C and Mo-N-C/$Ti_3C_2T_x$ heterostructure. The Fermi level is set to zero.

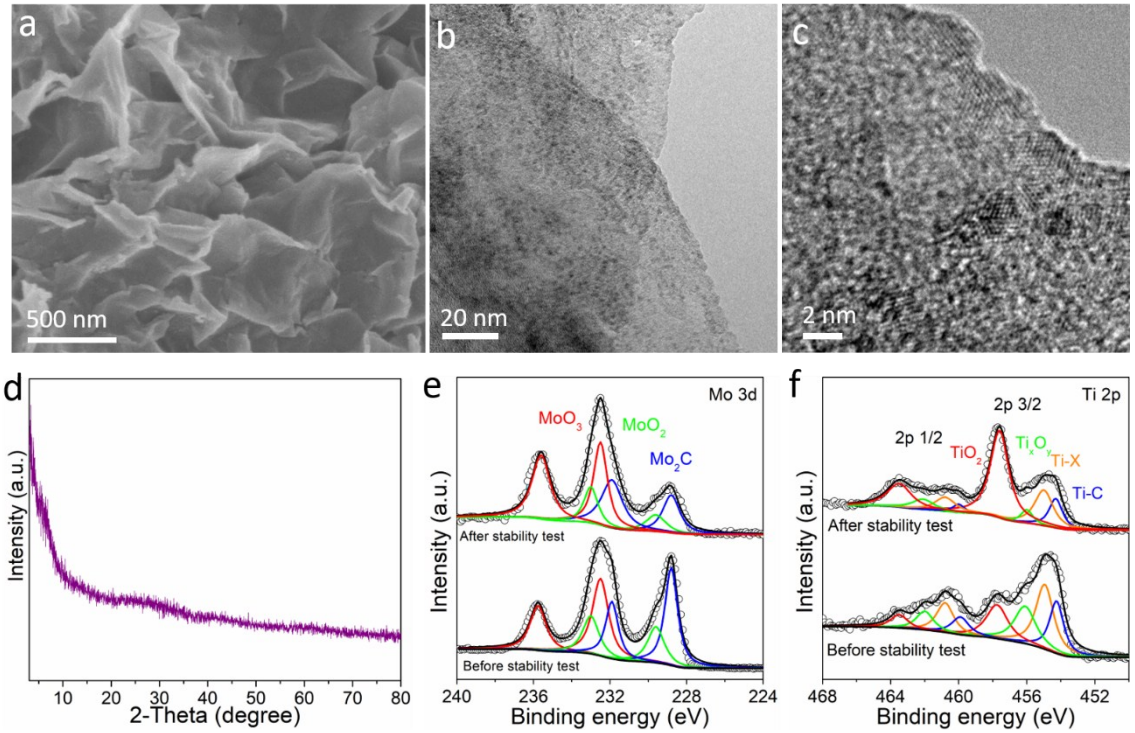

Fig. S21. (a) SEM image, (b, c) TEM images, (d) XRD pattern, (e) Mo 3d XPS and (f) Ti 2p XPS spectra of $Mo_2C/Ti_3C_2T_x$@NC after stability test.

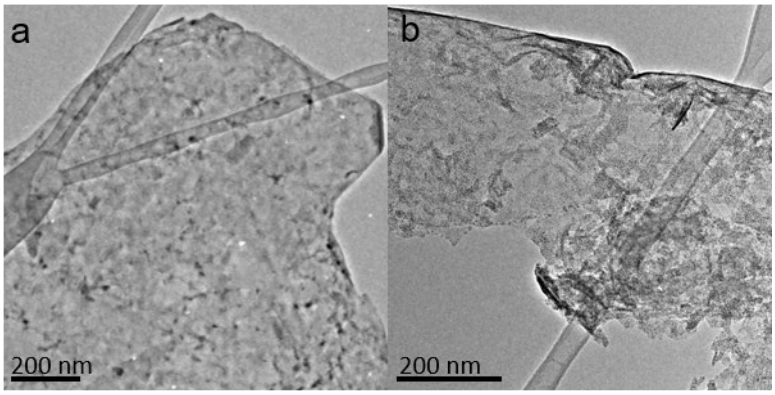

Fig. S22. TEM images of (a) M-650 and (b) M-850.

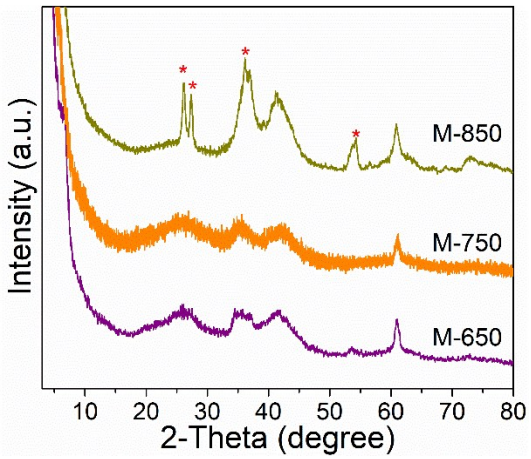

Fig. S23. XRD patterns of M-650, M-750 and M-850.. The observation of TiO_2 signal in XRD pattern implies the MXene is narrowly oxidized at higher temperature (850 ^{o}C).

Table S1. Comparison of HER performance for different electrocatalysts in 0.5 M H_2SO_4.

Catalyst	η_{10} [a] (mV)	b [b] (mV dev^{-1})	j_0 [c] (mA cm^{-2})	m [d] (mg cm^{-2})	Ref.
$Mo_2C/Ti_3C_2T_x$@NC	53	40	0.52	0.285	This work
MoC-Mo_2C/PNCDs	121	60	0.15	0.4	[8]
Mo_2C/NrGO	62	57	1.188	0.2	[9]
Mo/Mo_2C-HNS	89	70.72	n.a.[e]	0.285	[10]
Mo_2N-Mo_2C/HGr	157	55	0.062	0.337	[11]
Mo-Mo_2C	150	55	0.019	0.38	[12]
N-Mo_2C nanobelts	140	51.3	0.021	0.5	[13]
Mo_2C/VC@C	122	43.8	n.a.	0.28	[14]
Ni-Mo_2C@C	72	65.6	n.a.	0.531	[15]
Mo_2C@GC	125	66	n.a	0.2	[16]
P-Mo_2C@C	89	42	0.18	1.3	[17]
N-Mo_2C NSs	99	44.5	0.1	0.357	[18]
Mo_2C@C	141	56	0.029	0.9	[19]
Mo_2C@NPC/NPRGO	34	33.6	1.09	0.14	[20]
Mo_2C/NCF	144	55	n.a.	0.28	[21]
Mo_2C@NC	124	60	0.096	0.28	[22]
β-Mo_2C nanotubes	172	62	0.017	0.75	[23]
Mo_2CT_x MXene	189	70	<0.1	1	[24]
$Mo_2TiC_2T_x$-Pt_{SA}	30	30	1.54	1	[25]
$MoS_2/Ti_3C_2T_x$	152	70	0.6165	0.286	[26]
$Pt_{3.21}Ni@Ti_3C_2T_x$	18.55	13.3	2.62	n.a.	[27]
$Ti_3C_2T_x$ NFs	169	90	0.36	0.3	[28]
N-Ti_2CT_x	215	67	n.a.	0.178	[29]
$MoS_2/Ti_3C_2T_x$@C	135	45	0.029	0.4	[30]
Co-SACs	230	90	0.0388	0.2	[31]
VN@Ni_3N-Ni	129	79	n.a.	n.a.	[32]
CoP/Co-MOF	27	43	n.a.	5	[33]
1T'-ReSSe QDs	84	50.1	n.a.	n.a.	[34]
$Mo_{0.5}W_{0.5}S_2$	138	55	0.114	0.2	[35]
Ni-C-N NSs	60.9	32	0.0136	0.2	[36]
C shelled FeP/C	71	52	n.a.	0.2475	[37]

[a] overpotential at current density of 10 mA cm^{-2};
[b] Tafel slope;
[c] exchange current density;
[d] mass loading of catalysts on working electrode;
[e] not applicable

References

[1] P. E. Blöchl, *Phys. Rev. B,* 1994, **50**, 17953.
[2] G. Kresse and J. Furthmüller, *Comp. Mater. Sci.,* 1996, **6**, 15.
[3] G. Kresse and D. Joubert, *Phys. Rev. B,* 1999, **59**, 1758.
[4] S. Grimme, J. Antony, S. Ehrlich and H. Krieg, *J. Chem. Phys.,* 2010, **132**, 154104.
[5] H. Ang, H. Wang, B. Li, Y. Zong, X. Wang and Q. Yan, *Small* 2016, **12**, 2859.
[6] C. C. McCrory, S. Jung, I. M. Ferrer, S. M. Chatman, J. C. Peters and T. F. Jaramillo, *J. Am. Chem. Soc.,* 2015, **137**, 4347.
[7] J. D. Benck, T. R. Hellstern, J. Kibsgaard, P. Chakthranont and T. F. Jaramillo, *ACS Catal.,* 2014, **4**, 3957.
[8] X. F. Lu, L. Yu, J. Zhang and X. W. Lou, *Adv. Mater.,* 2019, **31**, 1900699.
[9] Z. Zhou, Z. Yuan, S. Li, H. Li, J. Chen, Y. Wang, Q. Huang, C. Wang, H. E. Karahan and G. Henkelman, *Small,* 2019, **15**, 1900358.
[10] J. Xiong, J. Li, J. Shi, X. Zhang, N.-T. Suen, Z. Liu, Y. Huang, G. Xu, W. Cai and X. Lei, *ACS Energy Lett.,* 2018, **3**, 341.
[11] H. Yan, Y. Xie, Y. Jiao, A. Wu, C. Tian, X. Zhang, L. Wang and H. Fu, *Adv. Mater.,* 2018, **30**, 1704156.
[12] J. Dong, Q. Wu, C. Huang, W. Yao and Q. Xu, *J. Mater. Chem., A* 2018, **6**, 10028.
[13] S. Jing, L. Zhang, L. Luo, J. Lu, S. Yin, P. K. Shen and P. Tsiakaras, *Appl. Catal. B: Environ.,* 2018, **224**, 533.
[14] C. Huang, X. Miao, C. Pi, B. Gao, X. Zhang, P. Qin, K. Huo, X. Peng and P. K. Chu, *Nano Energy,* 2019, **60**, 520.
[15] F. Yu, Y. Gao, Z. Lang, Y. Ma, L. Yin, J. Du, H. Tan, Y. Wang and Y. Li, *Nanoscale,* 2018, **10**, 6080.
[16] J. Zhu, Y. Yao, Z. Chen, A. Zhang, M. Zhou, J. Guo, W. D. Wu, X. D. Chen, Y. Li and Z. Wu, *ACS Appl. Mater. Interfaces,* 2018, **10**, 18761.
[17] Z. Shi, K. Nie, Z.-J. Shao, B. Gao, H. Lin, H. Zhang, B. Liu, Y. Wang, Y. Zhang and X. Sun, *Energy Environ. Sci.,* 2017, **10**, 1262.
[18] J. Jia, T. Xiong, L. Zhao, F. Wang, H. Liu, R. Hu, J. Zhou, W. Zhou and S. Chen, *ACS Nano,* 2017, **11**, 12509.
[19] Y.-Y. Chen, Y. Zhang, W.-J. Jiang, X. Zhang, Z. Dai, L.-J. Wan and J.-S. Hu, *ACS Nano,* 2016, **10**, 8851.
[20] J.-S. Li, Y. Wang, C.-H. Liu, S.-L. Li, Y.-G. Wang, L.-Z. Dong, Z.-H. Dai, Y.-F. Li and Y.-Q. Lan, *Nat. Commun.,* 2016, **7**, 11204.
[21] Y. Huang, Q. Gong, X. Song, K. Feng, K. Nie, F. Zhao, Y. Wang, M. Zeng, J. Zhong and Y. Li, *ACS Nano,* 2016, **10**, 11337.
[22] Y. Liu, G. Yu, G. D. Li, Y. Sun, T. Asefa, W. Chen and X. Zou, *Angew. Chem. Int. Ed.,* 2015, **54**, 10752.
[23] F. X. Ma, H. B. Wu, B. Y. Xia, C. Y. Xu and X. W. Lou, *Angew. Chem. Int. Ed.,* 2015, **54**, 15395.
[24] Z. W. Seh, K. D. Fredrickson, B. Anasori, J. Kibsgaard, A. L. Strickler, M. R. Lukatskaya, Y. Gogotsi, T. F. Jaramillo and A. Vojvodic, *ACS Energy Lett.,* 2016, **1**, 589.
[25] J. Zhang, Y. Zhao, X. Guo, C. Chen, C.-L. Dong, R.-S. Liu, C.-P. Han, Y. Li, Y. Gogotsi and G. Wang, *Nat. Catal.,* 2018, **1**, 985.

[26] J. Liu, Y. Liu, D. Xu, Y. Zhu, W. Peng, Y. Li, F. Zhang and X. Fan, *Appl. Catal. B: Environ.,* 2019, **241**, 89.
[27] Y. Jiang, X. Wu, Y. Yan, S. Luo, X. Li, J. Huang, H. Zhang and D. Yang, *Small,* 2019, **15**, 1805474.
[28] W. Yuan, L. Cheng, Y. An, H. Wu, N. Yao, X. Fan and X. Guo, *ACS Sustain. Chem. Eng.,* 2018, 6, 8976.
[29] Y. Yoon, A. P. Tiwari, M. Lee, M. Choi, W. Song, J. Im, T. Zyung, H.-K. Jung, S. S. Lee and S. Jeon, *J. Mater. Chem. A,* 2018, **6**, 20869.
[30] X. Wu, Z. Wang, M. Yu, L. Xiu and J. Qiu, *Adv. Mater.,* 2017, **29**, 1607017.
[31] M. D. Hossain, Z. Liu, M. Zhuang, X. Yan, G. L. Xu, C. A. Gadre, A. Tyagi, I. H. Abidi, C. J. Sun and H. Wong, *Adv. Energy Mater.,* 2019, **9**, 1803689.
[32] X. Dong, H. Yan, Y. Jiao, D. Guo, A. Wu, G. Yang, X. Shi, C. Tian and H. Fu, *J. Mater. Chem. A,* 2019, **7**, 15823..
[33] T. Liu, P. Li, N. Yao, G. Cheng, S. Chen, W. Luo and Y. Yin, *Angew. Chem. Int. Ed.,* 2019, **58**, 4679.
[34] Z. Lai, A. Chaturvedi, Y. Wang, T. H. Tran, X. Liu, C. Tan, Z. Luo, B. Chen, Y. Huang and G.-H. Nam, *J. Am. Chem. Soc.,* 2018, **140**, 8563.
[35] H. Wang, L. Ouyang, G. Zou, C. Sun, J. Hu, X. Xiao and L. Gao, *ACS Catal.* 2018, **8**, 9529.
[36] J. Yin, Q. Fan, Y. Li, F. Cheng, P. Zhou, P. Xi and S. Sun, *J. Am. Chem. Soc.,* 2016, **138**, 14546.
[37] D. Y. Chung, S. W. Jun, G. Yoon, H. Kim, J. M. Yoo, K.-S. Lee, T. Kim, H. Shin, A. K. Sinha and S. G. Kwon, *J. Am. Chem. Soc.,* 2017, **139**, 6669.